Preprints of the 2012 20th Mediterranean Conference on Control & Automation (MED), Barcelona, Spain, July 3-6, 2012

Numerical studies of concentration estimation and source tracking of a gaseous source using multiple mobile distributed sensors

Michael A. Demetriou Nikolaos A. Gatsonis Jeffrey R. Court

***Abstract*— The objective of this work is to provide the performance-based guidance of multiple mobile sensing agents onboard air vehicles that are used for the state reconstruction associated with gaseous sources. A source is assumed to move freely in the spatial domain of interest and multiple sensing air vehicles (SAV) are employed to assess the effects of the moving source. A model-based estimation scheme is implemented in order to primarily estimate the effects (concentration) of the moving source with a secondary goal of estimating the proximity of the moving source. The proposed guidance scheme provides the spatial relocation of the SAVs based solely on the performance of the estimation scheme. Extensive numerical studies for both stationary and mobile sources are considered to provide a convincing argument on the performance-based guidance of mobile sensors.**

***Index Terms*— Plume dispersion; moving source; multiple mobile sensors; grid adaptation; performance-based guidance.**

I. Introduction

The objective of this study is to provide the guidance of multiple mobile sensors on board air vehicles (Sensing Air Vehicles) used to provide concentration estimates of contaminants in the atmosphere. We build upon our earlier efforts [1], [2], [3] and now consider multiple SAVs whose motion in 2D space is dictated by the performance of the state estimator associated with a moving gaseous source. A schematic depicting a typical situation with a moving gaseous source and multiple sensing agents onboard unmanned aircraft is given in Figure 1.

Unlike our earlier efforts, the current work considers a centralized estimator utilizing N mobile sensors (SAVs) whose guidance is given in terms of the performance of the state estimator, but no explicit collision avoidance is imposed. The reason for this application-specific relaxation of collision avoidance is because the very motion of SAV precludes any collision. This becomes clear when one considers the specifics of the guidance for each SAV; each SAV moves to spatial locations of larger state estimation errors as it implements a (spatial) gradient scheme. When an SAV occupies a spatial region with large estimation error, the error in the region begins to decrease and therefore any other SAV will have to move to regions with larger estimation error.

The physical modeling of a single species concentration due to a moving source is summarized in the next section. Sensor modeling along with the dynamics of typical unmanned air vehicles that would carry the sensing devices are presented in Section III. The proposed combined state estimation and multiple-SAV guidance are given in Section IV. A description of the numerical implementation scheme, which includes a sensor-based grid adaptation is summarized in Section V. Extensive numerical results are described in Section VI and conclusions follow in Section VII.

The authors are with Worcester Polytechnic Institute, Dept of Mechanical Engineering, Worcester, MA 01609, USA, {mdemetri,gatsonis,jeff.court}@wpi.edu. The authors gratefully acknowledge financial support from the AFOSR, grant FA9550-09-1-0469.

II. Physical Modeling

We are concerned with the release of a trace contaminant in the atmosphere within a bounded spatial domain $\Omega = [0, L_X] \times [0, L_Y] \subset \mathbb{R}^2$. The concentration $c(t, X, Y)$ at a given time and spatial location evolves according to the following atmospheric advection diffusion equation

$$\begin{aligned} &\frac{\partial c}{\partial t} + W_X \frac{\partial c}{\partial X} + W_Y \frac{\partial c}{\partial Y} = \frac{\partial}{\partial X}\left(\kappa_{XX} \frac{\partial c}{\partial X}\right) \\ &+ \frac{\partial}{\partial Y}\left(\kappa_{YY} \frac{\partial c}{\partial Y}\right) + S(t, X, Y) \\ &c\left(0, X, Y\right) = c_0\left(X, Y\right). \end{aligned} \tag{1}$$

The functions κ_{XX}, κ_{YY} denote the eddy diffusivities, W_X, W_Y are the wind velocities, and $S(t, X, Y)$ is a diffusive source term. Since it is assumed that the atmosphere is void of the trace contaminant, the boundary conditions are assumed to represent constant zero concentration $c|_{\partial\Omega} = 0$ [4], [5], [6].

A single contaminant source is assumed that admits the expansion $S(t, X, Y) = b\left(X, Y\right) f\left(t\right)$, where $b\left(X, Y\right)$ denotes the spatial distribution and $f\left(t\right)$ its release rate. In our

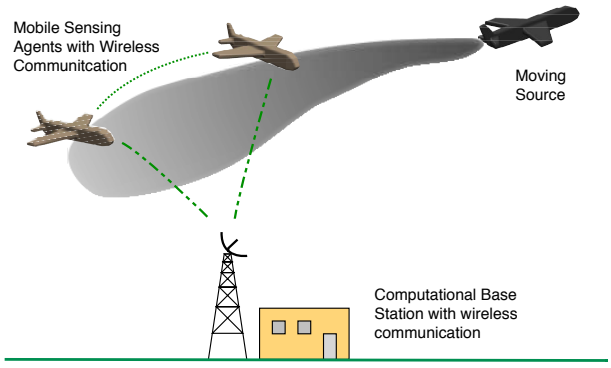

Fig. 1. Typical source detection problem with an intruder releasing a contaminant and a mobile sensor network seeking the source.

978-1-4673-2529-5/12/$31.00 ©2012 IEEE

study, it is further assumed that the spatial distribution of the source is a point source at the spatial point $(X_c, Y_c) \in \Omega$ and represented by the spatial Dirac delta function

$$b(X, Y) = \delta(X - X_c)\delta(Y - Y_c). \tag{2}$$

III. Sensor modeling

Concentration measurements are provided by multiple sensors on board sensing aerial vehicles. It is assumed that the SAVs used are fixed wing aircraft equipped with navigation capabilities and with concentration sensors. The SAVs can provide process state information for concentration measurement $c(t, X, Y)$ as well as concentration gradient measurements $\frac{\partial c(t,X,Y)}{\partial X}, \frac{\partial c(t,X,Y)}{\partial Y}$ in each of the spatial directions at the sensor locations (X_{si}, Y_{si}), $i = 1, \ldots, N$

$$y_i(t) = c(t, X_{si}, Y_{si}) = \int_0^{L_X}\int_0^{L_Y} \delta(X - X_{si})\delta(Y - Y_{si})c(t, X, Y)\, dX\, dY. \tag{3}$$

A. Mobile sensing agent dynamics and control

The performance-based guidance scheme considered here provides a desired control input signal to each of the SAVs. It is assumed that each SAV has knowledge of its full state $(X_i(t), Y_i(t), \psi_i(t))$, $i = 1, \ldots .N$. For a fixed wing aircraft as depicted in Figure 2, having a standard low level autopilot [7], the dynamic equations of motion for a 2D plane parallel to the ground is given by [8], [9]

$$\begin{bmatrix} M\ddot{X} \\ M\ddot{Y} \\ I\ddot{\psi} \end{bmatrix} = \begin{bmatrix} \cos\psi & 0 \\ \sin\psi & 0 \\ 0 & 1 \end{bmatrix} \begin{bmatrix} \tau_l \\ \tau_a \end{bmatrix} + \begin{bmatrix} -M\omega_\psi v \sin\psi \\ M\omega_\psi v \cos\psi \\ 0 \end{bmatrix} \tag{4}$$

where v denotes the forward aircraft speed and ω_ψ is its turning rate. The aircraft control inputs are the *thrust* τ_l and *angular turning force* τ_a. Included in the above is the assumption that the autopilot factors in the appropriate drag forces and therefore the inputs are resultant forces that act in order to move the SAV. When the input forces are set to zero, the SAV speed and turning rate remain unchanged and thus the aircraft will maintain constant speed and angular turning rate. The mass matrix is given by $\mathcal{M} = \text{diag}\ \{M, M, I\}$ where M denotes the SAV mass and I its moment of inertia. The motion constrains of the SAVs are similar to those of terrain vehicles, but the SAVs are additionally subjected to physical constraints limiting their forward speed and v turning rate $\dot{\psi}$ $v_{min} \leq v \leq v_{max}$, $-\omega_{\psi,max} \leq \omega_\psi \leq \omega_{\psi,max}$.

For an aircraft equipped with a lower level autopilot [10], [7], the pose of the sensor may be described by the kinematic equations [11]

$$\dot{X}(t) = v(t)\cos(\psi(t)), \dot{Y}(t) = v(t)\sin(\psi(t)), \dot{\psi}(t) = \omega_\psi(t),$$

where the pose is represented by the Cartesian position (X, Y) and the SAV's heading angle ψ. The motion is determined by the SAV's speed and angular turning rate $(v(t), \omega_\psi(t))$ as shown in Figure 2. The above equation can be expressed in matrix form $\dot{\mathbf{q}}(t) = \mathbf{S}(t)\mathbf{v}(t)$ where

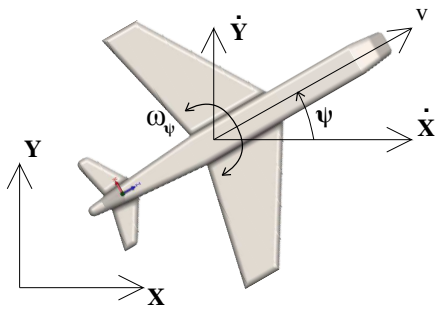

Fig. 2. Schematic of the SAV coordinate system in 2D.

$\dot{\mathbf{q}}(t) = \left[\dot{X}(t), \dot{Y}(t), \dot{\psi}(t)\right]^T$, $\mathbf{v}(t) = \left[v(t), \dot{\psi}(t)\right]^T$, and the transformation matrix $\mathbf{S}(t)$ is

$$\mathbf{S}(t) = \begin{bmatrix} \cos(\psi) & 0 \\ \sin(\psi) & 0 \\ 0 & 1 \end{bmatrix}.$$

The equation of motion (4) can be rewritten in matrix form

$$\mathcal{M}\ddot{\mathbf{q}} = \mathcal{B}_1\tau - \mathbf{A}^T\lambda.$$

Substituting the kinematic equation into the dynamic equation, yields

$$\mathcal{M}(\dot{\mathbf{S}}\mathbf{v}) = \mathcal{B}_1\tau - \mathbf{A}^T\lambda \Rightarrow \mathcal{M}\mathbf{S}\dot{\mathbf{v}} + \mathcal{M}\dot{\mathbf{S}}\mathbf{v} = \mathcal{B}_1\tau - \mathbf{A}^T\lambda$$

Premultiplying by $\mathbf{S}^T$ yields

$$\mathbf{S}^T\mathcal{M}\mathbf{S}\dot{\mathbf{v}} + \mathbf{S}^T\mathcal{M}\dot{\mathbf{S}}\mathbf{v} = \mathbf{S}^T\mathcal{B}_1\tau - \mathbf{S}^T\mathbf{A}^T\lambda$$

The equation can be simplified with the introduction of the transformed mass matrix $\mathcal{M}_1 = \mathbf{S}^T\mathcal{M}\mathbf{S} = \text{diag}\{M, I\}$. The term $\mathbf{S}^T\mathcal{M}\dot{\mathbf{S}}$ is simplified to $\mathbf{S}^T\mathcal{M}\dot{\mathbf{S}} = \mathbf{0}_{2\times1}$. The input control matrix $\mathcal{B}_2$ is also simplified to $\mathcal{B}_2 = \mathbf{S}^T\mathcal{B}_1 = \mathbf{I}_{2\times2}$. As a consequence of the premultiplication by $\mathbf{S}^T$, the constraint matrix is eliminated from above since $\mathbf{S}^T\mathbf{A}\lambda = \mathbf{0}_{2\times1}$. For the inputs $\tau = [\tau_l, \tau_a]$, the dynamic equation of motion can then be written as

$$\mathcal{M}_1\dot{\mathbf{v}}_i = \tau_i, \ \ i = 1, \ldots, N. \tag{5}$$

This is the equation that will be used in conjunction with the estimator dynamics in order to arrive at SAV control inputs that are solely dictated by estimator performance.

IV. State estimation with mobile distributed sensors

We utilize the estimation scheme presented in [12]. However, unlike the earlier similar works [1], [2], [3], we utilize multiple SAVs in a centralized estimation scheme with a modified guidance controller. We summarize the estimation scheme and provide only the details concerning the guidance of the multiple SAVs.

The process state estimate $\widehat{x}$ is governed by an evolution equation in the Hilbert space $\mathcal{X} = L^2(\Omega)$

$$\begin{aligned}\dot{\widehat{x}}(t) = \mathcal{A}\widehat{x}(t) - \sum_{i=1}^{N} \gamma_i \mathcal{C}^*(\theta_{si}(t))\mathcal{C}(\theta_{si}(t))\widehat{x}(t) \\ + \sum_{i=1}^{N} \gamma_i \mathcal{C}^*(\theta_{si}(t)) y_i(t;\theta_{si}(t)), \quad \widehat{x}(0) = 0,\end{aligned} \tag{6}$$

where $\mathcal{A}$ is the advection diffusion operator associated with (1), $\mathcal{C}$ is the output operator representing the sensor spatial distribution in (3) and y is the N dimensional vector of sensor data. The gains $\gamma_i > 0$ are taken to be the same for all $i = 1, \ldots, N$ and $\theta_{si}(t) = (X_{si}, Y_{si})$ is the Cartesian position of the i^{th} sensor.

A. Mobile sensing vehicle guidance

The guidance scheme presented here is a 2D version of that presented in our earlier work [3]. It is based on Lyapunov methods and includes the norm of the state estimation error and the kinetic energy of each of the SAVs

$$\begin{aligned}V = -\langle e(t), \mathcal{A}_{cl}(X(t), Y(t))e(t)\rangle_{\mathcal{X}} \\ + \sum_{i=1}^{N} \left(\frac{1}{2} \mathbf{v}_i^T(t) \mathcal{M}_1 \mathbf{v}_i(t) \right),\end{aligned} \tag{7}$$

where $\mathcal{A}_{cl}(X(t), Y(t)) = \mathcal{A} - \sum_{i=1}^{N} \gamma_i \mathcal{C}^*(\theta_{si}(t))\mathcal{C}(\theta_{si}(t))$. Forcing its time derivative to be negative definite, one arrives at the following guidance laws

$$\tau_i = -\mathbf{S}^T \begin{bmatrix} \varepsilon_i \varepsilon_{X_i} & \varepsilon_i \varepsilon_{Y_i} & 0 \end{bmatrix}^T, \; i = 1, \ldots, N,$$

where $\varepsilon_i(t)$ denotes the output estimation error at the location of the i^{th} sensor, and $\varepsilon_{Xi}, \varepsilon_{Yi}$ denote the spatial gradients of the output estimation error in the X and Y directions at the current location of the i^{th} sensor. The above control law only provides input for the Cartesian coordinates, via the thrust control torque τ_{li}. To address the angular torque control signal τ_{ai}, a two-level motion controller is implemented whereby the angular torque τ_{ai} is chosen as a function of the two Cartesian torques; these torques are the X and Y components of the thrust control torque τ_{li} defined above.

V. Numerical implementation

The simulations presented in this work are run in two parts. First, sensor data is generated by solving the advection diffusion equation with a high dimensional system, and that would serve in place of experimental data. The solution for a known source trajectory is stored to a data file at every time step. This first part of the simulation is done a priori and could be omitted in the presence of experimental data. The second part of the simulation is the actual state estimation that must be done in real time. Here, small portions of sensor data are read from the stored data files based on the location of the sensor at that time step.

A. Finite dimensional approximation of the plant and state estimator

For discrete computations, a finite volume approach is implemented to discretize the computational domain [13]. A uniform high dimensional grid is implemented on the forward problem to provide a high fidelity solution. The estimator uses a switching approach in which multiple stretched grids of low dimension are calculated a priori. This allows the computation of the estimator to be done in real time. A detailed description of the grid discretization and adaptation is available in our previous work [1], [2], [3].

VI. Computational results

The forward problem is simulated with a 90×90 computational grid over the spatial domain Ω =[0,4km]$\times$ [0,4km]. The reduced dimensional estimation is implemented with a 30×30 grid. Grid adaptation in the form of switching is implemented on the estimator grid, similar to our earlier works [2], [3]. In order for this switching adaptation to be implemented with multiple sensors and a single estimator, an area of highest interest must be chosen in which to focus the grid. As a first approach, the sensor that was measuring a higher concentration was chosen to be the focus of the refined area of the adapted grid.

A. Stationary source

A stationary source is placed in the center of the spatial domain at (2km,2km) and releases material at a constant rate. The atmospheric advection in the domain is taken to be 5m/s North and 5m/s East. The diffusivity of the material is 20m^2/s. Both sensors onboard two SAVs start patrolling in the North East area of Ω. They initiate a patrolling behavior and exit that behavior when they individually sense a nonzero concentration. Upon receiving a non-zero measurement (i.e. above a certain lower-level threshold) they activate the implementation of the proposed state estimator.

Figure 3 depicts the trajectory of the two sensors while estimating a stationary source. The sensor starting further to the left detects a nonzero concentration first and begins estimating the state. Soon after, the second sensor detects a nonzero concentration. Since the second sensor was physically close to the first sensor and the first sensor reduced the state estimation error in its proximity, the second sensor starts heading away from the first sensor towards areas of higher interest (i.e. of higher state estimation error). Eventually, both sensors converge on the source location, where the state estimation error is highest in the spatial domain. Figure 4 depicts the trajectory of a single sensor for comparison.

Figure 5 shows the distance of the sensors from the source throughout the duration of the study. Initially, the sensors are placed fairly close to one another, separated by 150m. Since both sensors are downwind of the source, naturally the sensor closer to the source would detect the source first. Around 110s, the second sensor detects a nonzero concentration and begins tracking the plume. The distance plot demonstrates that the second sensor does not initially head towards the source. This is because that region of the domain was

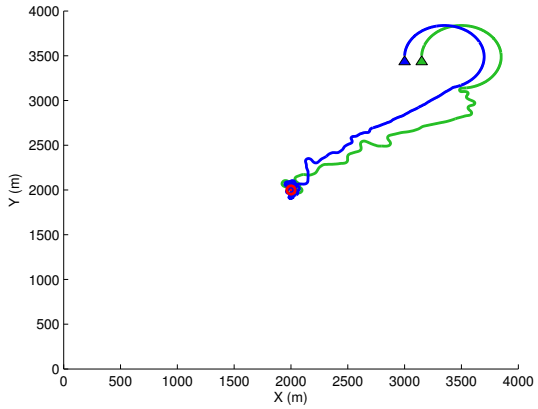

Fig. 3. Stationary source: trajectories of two SAVs.

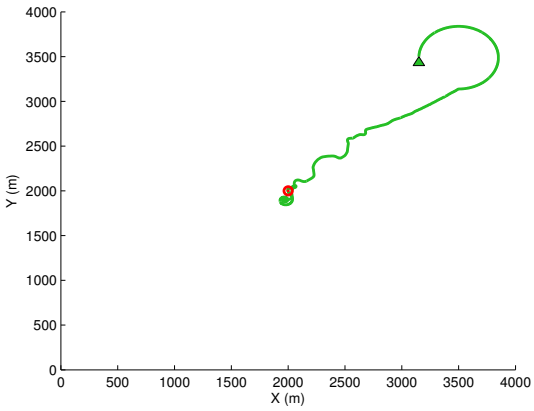

Fig. 4. Stationary source: trajectory of single SAV.

recently estimated by the first sensor, leaving other areas with higher estimation error. Eventually, both sensors travel very close to the source, where a large estimation error is continuously introduced by the source term.

Figure 7 shows the error norm for the case of a single sensor (blue) and the case of two sensors (red) for a stationary source. Considering the single sensor case, it can be seen that around 160s, the sensor detects the plume and starts reducing the error. Around 225s, the sensor overshoots the source and loses the plume. While it is out of the plume, the norm of the state error starts increasing since the sensor is not measuring a non zero estimation error. At approximately 280s, the sensor again finds the plume and starts reducing the state estimation error. The multiple sensor case shows that the error is reduced faster than it was with a single sensor. This is to be expected, since the estimation scheme has more information about the actual concentration state. The plot also demonstrates that when one of the two SAVs misses the plume, the norm of the state estimation error is not affected as drastically as it is with the single SAV case.

Simulations are conducted on a 5 node Linux cluster running Red Hat 3.4.6. The serial code is implanted on one of the nodes with a Quad Core Intel Xeon processor clocked at 2.33GHz with 16GB of RAM. The code is compiled with Intel's Fortran compiler, IFORT version 9.0. For the stationary source, the computational time for a single sensor is approximately 140s for 300s of simulation. The addition of a second sensor increased the computational time to approximately 150s for 300s of simulated results. It should be noted that these computational times include outputting significant amounts of visualization data that would not be necessary in a real world implementation. This demonstrates that increasing the number of sensors provides a significantly improved state estimate, and only a slight increase in computational requirements.

B. Diagonal Source Trajectory

A diagonal source trajectory is used to demonstrate the performance of the system with a mobile source. The source

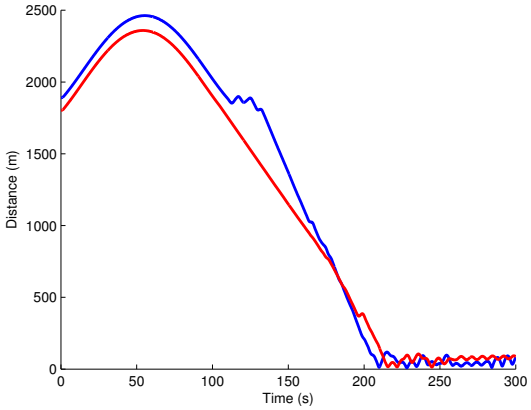

Fig. 5. Stationary source: evolution of two SAV distances from source.

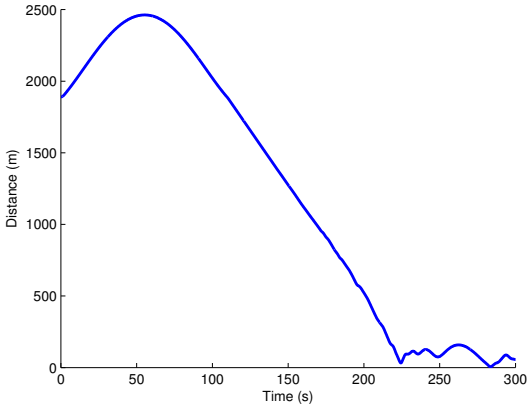

Fig. 6. Stationary source: evolution of single SAV distance from source.

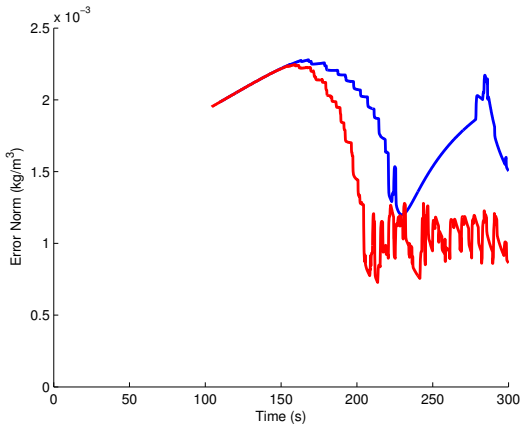

Fig. 7. Stationary source: evolution of state error L_2 norm for single (blue) and two SAVs (red).

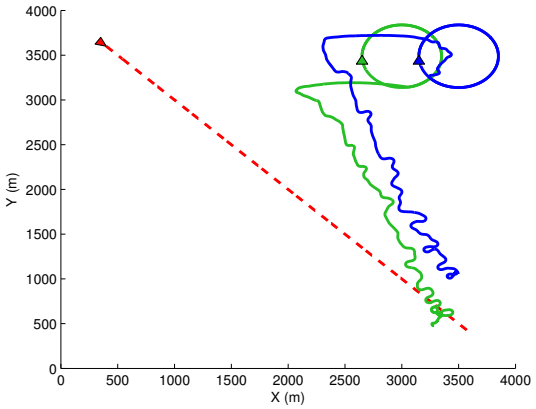

Fig. 8. Diagonal source trajectory: trajectories of two SAVs.

releases material at a constant rate, starting at the top left of the domain and traveling to the bottom right of the domain. It travels with a constant velocity of approximately 15m/s. The atmospheric advection is taken to be 5m/s North and 5m/s East and diffusivity is assumed constant at 20m^2/s. Two SAVs are employed to detect the source. The sensors patrol the North East part of the domain until they detect a nonzero concentration, at which time they begin estimating the state based on the guidance laws presented.

For a source moving across the domain, the trajectory for two SAVs is shown in Figure 8. As is expected, the SAV closer to the source (red) detects the source first and begins heading towards areas of higher estimation error. The second SAV behaves similar to the one from the stationary case. Initially, the SAV does not travel towards the source location since the first SAV has reduced the state estimation error in such a way to make areas further from the source of more interest. However, the SAV soon reduces the state errors in those areas and heads towards the location of the first SAV and moving source. Similarly, Figure 8 depicts the trajectory for the single SAV case. It should be noted that the single SAV trajectory is not identical to that of the two SAVs.

Figure 10 shows the distance of the SAVs from the source location over time. Again, one SAV starts closer (red), so it heads towards the source location right away. The second SAV ends up moving away from the source momentarily towards areas of higher interest, but eventually heads towards the source location. Figure 11 provides the single SAV case.

The computational time for the moving source was approximately 180s for a 500s simulation. Adding a second SAV to the simulation increased the computational time to 200s for a 500s simulation.

C. Crossing Source Trajectory

Figure 12 shows the results for a crossing source that is tracked by $N = 3$ sensors. The atmospheric parameters are the same as in the other cases, with a longer simulation time to account for the longer trajectory of the source. The three SAVs are set up in a configuration such that

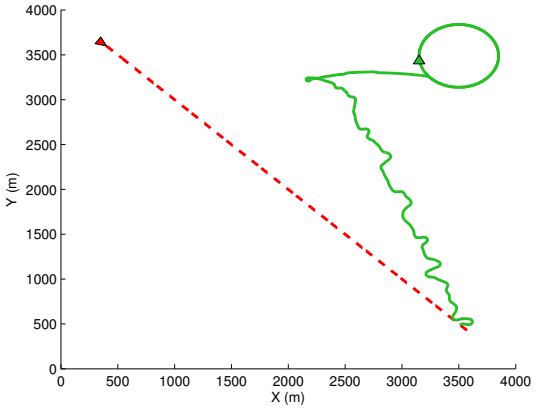

Fig. 9. Diagonal source trajectory: trajectory of a single SAVs.

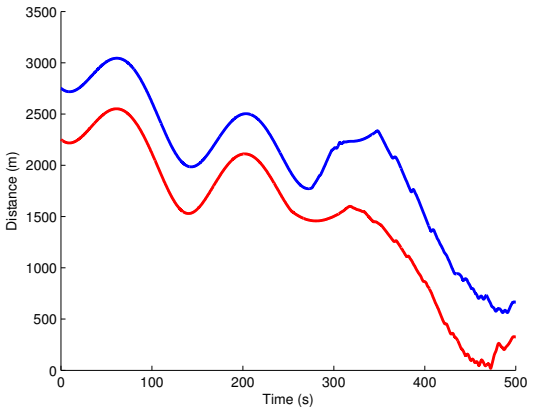

Fig. 10. Diagonal source trajectory: evolution of two SAV distances from source.

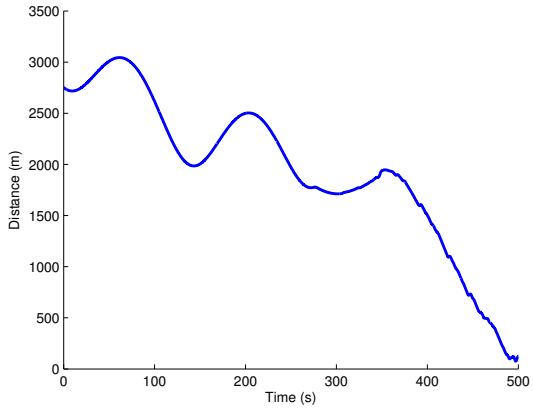

Fig. 11. Diagonal source trajectory: evolution of a single SAV distance from source.

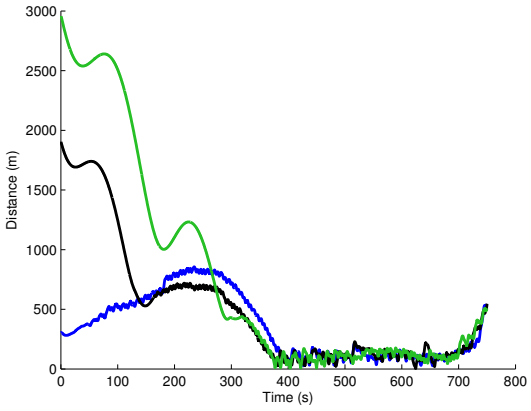

Fig. 13. Crossing source trajectory: evolution of three SAV distances from source.

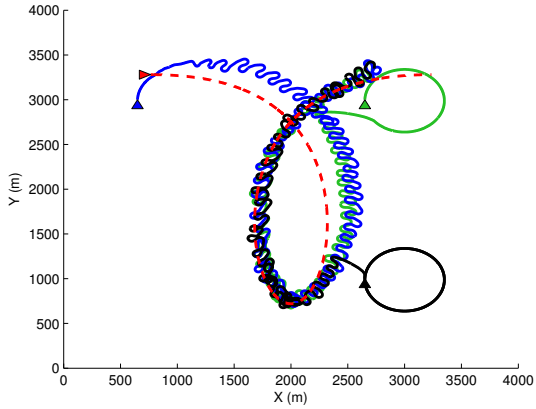

Fig. 12. Crossing source trajectory: trajectories of three SAVs.

each one patrols a different region. The first SAV begins patrolling close to the source location, so it detects the source very quickly. The two remaining SAVs detect the contaminant at a later time when the source comes near to their patrol region. Due to the continuous nature of the release, a large state estimation error is created near the source's location, creating an area of interest for the SAVs. The distance of the SAVs from the source can be seen in Figure 13, where all of the SAVs tend to converge on the source location. The sudden increase of the distance at around t=720s can be attributed to the fact that the source is moving leeward (northeasterly direction) and the SAVs cannot obtain significant concentration measurements as they are positioned windward of the source.

VII. Conclusions

This work considered the use of multiple SAVs for the concentration estimation due to a moving gaseous source. Using a model-based estimator scheme, a Lyapunov-based law provided the guidance of the SAVs in terms of the control torques. The motion control signals for each of the SAVs were expressed in terms of the state estimation error and its spatial gradients, and essentially moved the mobile sensors in spatial locations of larger estimation errors. Due to the specific nature of the guidance laws, there was no explicit need to impose collision avoidance.

Extensive numerical studies for both stationary and moving sources provided an insight on the use of mobile sensors for the estimation of spatially distributed processes.

References

[1] M. A. Demetriou, N. A. Gatsonis, and J. R. Court, "Numerical investigation of the spatial estimation error in sensor guidance used for the localization of a gaseous source in a 2D domain," in *Proc. of the 19th Mediterranean Conference on Control and Automation*, Corfu, Greece, June 20-23 2011, pp. 1386 –1391.

[2] ——, "Model-based detection of a moving gaseous source in a 2D spatial domain using a sensor-based grid adaptation approach," in *Proc. of the 2011 American Control Conf.*, San Francisco, CA, June 29- July 1 2011, pp. 2374–2380.

[3] ——, "Lyapunov based guidance of a mobile sensing agent for state estimation of a gaseous source in a 3D spatial domain," in *Proc. of the 50th IEEE Conference on Decision and Control*, Orlando, FL, December 12-15 2011.

[4] J. H. Seinfeld and S. N. Pandis, *Atmospheric Chemistry and Physics: From Air Pollution to Climate Change*. New York: Wiley-Interscience, 2006.

[5] S. P. Arya, *Air Pollution Meteorology and Dispersion*. New York: Oxford University Press, 1999.

[6] R. A. Dobbins, *Atmospheric Motion and Air Pollution*. New York: Wiley, 1979.

[7] R. Fierro and F. Lewis, "Control of a nonholonomic mobile robot: Backstepping kinematics into dynamics," *Journal of Robotic Systems*, vol. 14(3), pp. 149–164, 1997.

[8] B. Etkin, *Dynamics of Flight*. New York: Wiley, 1996.

[9] B. Stevens and F. Lewis, *Aircraft Control and Simulation*. London: J. Wiley, 2003.

[10] W. Ren and R. W. Beard, "Trajectory tracking for unmanned air vehicles with velocity and heading rate constraints," *IEEE Tr. on Contr. Sys. Tech.*, vol. 12(5), pp. 706–716, Sept. 2004.

[11] ——, "CLF-based tracking control for UAV kinematic models with saturation constraints," in *Proc. of the 42nd IEEE Conference on Decision and Control*, Maui, HI, December 2003.

[12] M. A. Demetriou, "Guidance of mobile actuator-plus-sensor networks for improved control and estimation of distributed parameter systems," *IEEE Tr. on Automatic Control*, vol. 55(7), pp. 1570–1584, 2010.

[13] C. Hirsch, *Numerical Computation of Internal & External Flows*. Oxford, GB: Butterworth-Heinemann, 2007.